Journal of Controlled Release 341 (2022) 80–94

Contents lists available at ScienceDirect

Journal of Controlled Release

journal homepage: www.elsevier.com/locate/jconrel

Fabricating scalable, personalized wound dressings with customizable drug loadings via 3D printing

Jia Heng Teoh [a], Sook Muay Tay [b], Jerry Fuh [c], Chi-Hwa Wang [a,*]

[a] Department of Chemical and Biomolecular Engineering, National University of Singapore, 117585, Singapore
[b] Department of Surgical Intensive Care, Division of Anaesthesiology and Perioperative Medicine, Singapore General Hospital, Outram Road, 169608, Singapore
[c] Department of Mechanical Engineering, National University of Singapore, 117575, Singapore

ARTICLE INFO

Keywords:
3D printing
Hydrogel
Wound dressing
Personalized medicine
Drug delivery

ABSTRACT

In recent times, 3D printing has been gaining traction as a fabrication platform for customizable drug dosages as a form of personalized medicine. While this has been recently demonstrated as oral dosages, there is potential to provide the same customizability and personalization as topical applications for wound healing. In this paper, the application of 3D printing to fabricate hydrogel wound dressings with customizable architectures and drug dosages was investigated. Chitosan methacrylate was synthesized and mixed with Lidocaine Hydrochloride and Levofloxacin respectively along with a photoinitiator before being used to print wound dressings of various designs. These designs were then investigated for their effect on drug release rates and profiles. Our results show the ability of 3D printing to customize drug dosages and drug release rates through co-loading different drugs at various positions and varying the thickness of drug-free layers over drug-loaded layers in the wound dressing respectively. Two scale-up approaches were also investigated for their effects on drug release rates from the wound dressing. The influence that each wound dressing design has on the release profile of drugs was also shown by fitting them with drug release kinetic models. This study thus shows the feasibility of utilizing 3D printing to fabricate wound dressings with customizable shapes, drug dosage and drug release rates that can be tuned according to the patient's requirements.

1. Introduction

Wound dressings are ubiquitous in today's modern world and have benefitted mankind throughout history, going as far back as the prehistoric period [1]. Whenever an injury is inflicted on the skin, wound dressings serve as a viable and cost-effective treatment that protects the wound bed from the external environment and provides a moist wound environment that accelerates healing and reduces scarring [2]. Wound dressings also have a role to play even for serious skin injuries. Taking burns as an example, wound dressings continue to play a pivotal role in the treatment process alongside skin grafting, which is regarded as the gold standard of treatment. Wound dressings are effective in protecting the wound bed from the external environment during the administration of first aid shortly after the occurrence of the incident. While skin grafts are extracted and meshed in the case of autologous skin grafting or while they are being cultured in the case of cultured epithelial autografts [3], wound dressings can be utilized to help keep the wound bed moist and sterile, which leads to better graft take [4]. Wound dressings are also used to treat donor sites when autologous skin grafting is used and can also be used to protect the recipient site from mechanical shearing after grafting [5].

By incorporating active therapeutic agents into a wound dressing, its ability to facilitate wound healing can be augmented and additional functionalities such as treatment and prevention of infection can be added to improve patient care. As examples, antibiotics, antimicrobial peptides and metal nanoparticles such as silver [6–11], gold [12] or copper [13] nanoparticles can be incorporated to treat or prevent bacterial infections. Analgesics [14–16] or nonsteroidal anti-inflammatory drugs [17] can be added to reduce pain and growth factors [18,19], stem cells [20,21] or antioxidants [22,23] to accelerate tissue regeneration [24].

While wounds may appear in many shapes and sizes, depending on the cause of the injury, current over-the-counter wound dressings are not flexible enough to match the variability that wounds have. Trimming and overlapping of wound dressings are at times needed to cover the wound, leading to material wastage. While wound dressings with

* Corresponding author.
E-mail address: chewch@nus.edu.sg (C.-H. Wang).

https://doi.org/10.1016/j.jconrel.2021.11.017
Received 19 June 2021; Received in revised form 14 September 2021; Accepted 10 November 2021
Available online 15 November 2021

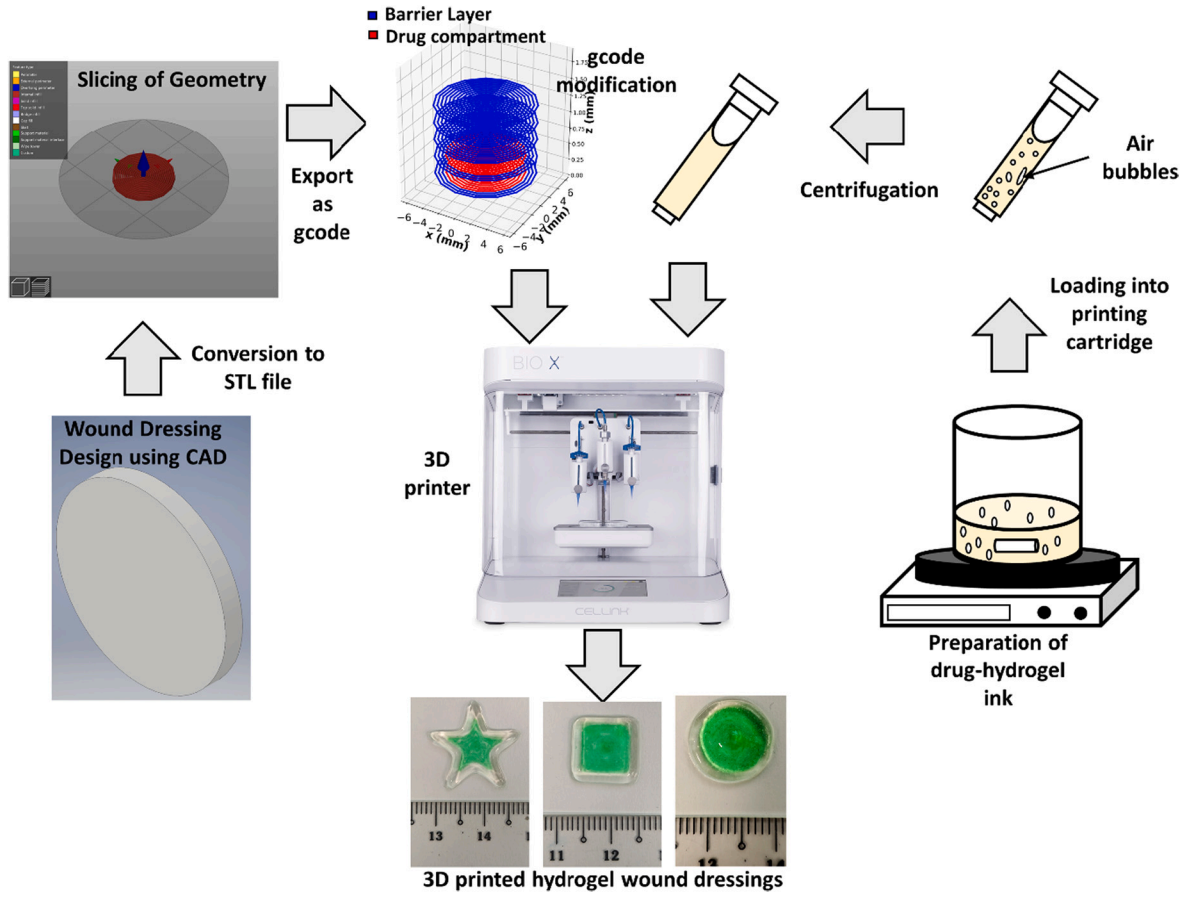

Scheme 1. Process scheme used for the fabrication of 3D printed hydrogel wound dressings in this study. For images of 3D printed hydrogel wound dressings, indocyanine green was only used to distinguish between the drug compartment and the barrier layer.

active formulations are present in the market, their respective compositions are fixed and cannot be tuned by end-users. Thus, 3D printing can be utilized as a solution to both these problems as a form of decentralized production, where health care providers can tune the size, shape and as mentioned above, the composition of the wound dressing to fit the personal needs of each patient [25].

3D printing is a technique that was initially used for the rapid prototyping of objects by depositing materials in a layer-by-layer manner [26]. Geometries of 3D printed structures can be designed first in a computer-aided design (CAD) software before it is exported as an STL file and converted into .gcode using a slicer software. This allows for the construction of wound dressings in a layer-by-layer fashion and thus, complex structures, which can help tune drug release rates from the wound dressing can be fabricated. While 3D printing traditionally utilizes thermoplastic filaments, softer materials such as hydrogels have also been shown to be compatible for 3D printing owing to their non-Newtonian behaviour. In recent times, the use of hydrogels to print biocompatible scaffolds for cells or to directly print various organs is becoming commonplace in literature [27–29]. Meanwhile, the fabrication of hydrogel-based wound dressings via 3D printing is gaining traction as well [30–33].

The use of 3D printing in fabricating drug delivery systems in the past decade is evident, mainly in the fabrication of solid oral dosages. Past studies have shown the ability of 3D printing to fabricate excipients that can control the release rate and profile of drugs out of tablets [34–39]. Spritam, being the first 3D printed drug product receiving FDA approval back in 2015 is also a testament to the success of 3D printing in personalizing oral dosages. While 3D printing was also previously used to fabricate wound dressings containing various active pharmaceutical ingredients [30–32,40–42], these wound dressings were isotropic in their respective designs and compositions and there has not been much investigation into the ability of 3D printing to customize drug release rates and profiles through its fabrication in a layer-by-layer manner.

In this study, we utilized 3D extrusion printing to print drug-loaded hydrogel wound dressings of various architectures. Taking the context of burns in our study, we have demonstrated the various drug release profile that can arise from these structures to adapt to various burn wounds. Wound dressings were first designed using CAD software before they were converted to .gcode using a slicer program. The .gcode was then further modified to allow for the position of drugs in the wound dressing to be customized. A 3D printer with multiple printheads was then used to create the wound dressing of different sizes, shapes and configurations using various drug-loaded hydrogels. The effect of wound dressing design on the release rate and profile of drugs from the wound dressing was investigated. We also investigated the scalability of wound dressings to accommodate different wound sizes and shapes. Release kinetic models were also fitted to the various drug release profiles obtained in this study.

2. Materials and methods

2.1. Materials

Low molecular weight chitosan, methacrylic anhydride and glacial acetic acid were used in the fabrication of chitosan methacrylate. The drugs used in this study were Lidocaine Hydrochloride (LIDHCl) and Levofloxacin (LVX). Lithium phenyl-2,4,6-trimethylbenzoylphosphinate (LAP) was used as a photoinitiator for the crosslinking of chitosan methacrylate. Phosphate buffered saline (Vivantis Technologies Sdn. Bhd., Malaysia) was used as the release medium for *in vitro* drug release

studies. Indocyanine green (Tokyo Chemical Industry Co., Ltd., Japan) was used to distinguish between different parts of the 3D printed architecture of the wound dressing. Acetonitrile was purchased from V.W. R, USA. Unless otherwise stated, all materials were purchased from Sigma Aldrich, USA.

We have prepared the hydrogel wound dressings in this study according to the workflow shown in Scheme 1.

2.2. Preparation of hydrogels

Chitosan methacrylate hydrogels used in this study were prepared according to the following protocol. Briefly, 3% (*w/v*) low molecular weight chitosan was dissolved in 3% (*v/v*) acetic acid under magnetic stirring and heating. Once dissolved, the temperature was set to 40 °C before methacrylate anhydride (1.5% (*v/v*)) was added and the mixture was allowed to stir for 3 h. The mixture was then dialyzed (MWCO = 12–14 kDa) for 5 days in DI water with the water changed twice a day. Dialyzed solutions were then frozen at -78 °C overnight and then lyophilized for 5 days.

2.3. Rheology

The rheological properties of chitosan methacrylate and drug-loaded chitosan methacrylate were characterized using a rotational rheometer (MCR-92 Anton Paar, USA). A 25 mm cone plate with an angle of elevation of 1° was used as the measuring geometry. Samples were first subjected to a pre-shear of 10 s^{-1} for 1 min to remove any existing structural artifacts before being allowed to equilibrate for 3 min before every run. The viscosity and shear stress as a function of shear rate was determined using steady-state flow tests in a range of 1–5000 s^{-1}. Using a constant strain of 1%, which is within the linear viscoelastic range of chitosan methacrylate, a frequency sweep from 10 to 0.1 Hz was carried out. For thixotropy tests, chitosan methacrylate samples were first subjected to a low shear rate of 1 s^{-1} for 60 s, followed by a high shear rate of 4000 s^{-1} for 10 s and back to a low shear rate of 1 s^{-1} for 180 s. The high shear rate used was selected based on the maximum shear rate exerted on chitosan methacrylate during the actual 3D printing process which was calculated using the following equation [43]:

$$\dot{\gamma}^n = \left[\frac{VR^2}{\left(\frac{n}{3n+1}\right)\left(R^{\frac{3n+1}{n}}\right)}\right]^n R \quad (1)$$

Where $\dot{\gamma}$ is the shear rate, V is the flow rate of chitosan methacrylate out of the nozzle during the 3D printing process, R is the radius of the nozzle outlet and n is the power law index obtained from fitting the non-Newtonian power law model to the viscosity-shear rate profile of chitosan methacrylate. It is assumed that the flow rate of chitosan methacrylate in the nozzle is uniform.

All tests were carried out at 24 °C. Rheological measurements were conducted in triplicates and results were expressed as mean±standard deviation.

Table 1
List of drug release kinetic models used to fit the various cumulative release profiles obtained in this study, along with definitions of their respective terms.

Release kinetic model name	Model equation	Term definitions
Zero-order	$\frac{Q}{Q_\infty} = k_0 t$	k_0 = Zero-order constant
First-order	$\frac{Q}{Q_\infty} = 1 - e^{-k_1 t}$	k_1 = First-order constant
Higuchi	$\frac{Q}{Q_\infty} = k_H\sqrt{t}$	k_H = Higuchi constant
Hixson-Crowell	$\sqrt[3]{1-\frac{Q}{Q_\infty}} = 1 - k_{HC}t$	k_{HC} = Hixson-Crowell constant
Korsmeyer-Peppas	$\frac{Q}{Q_\infty} = k_{KP}t^n$	k_{KP} = Korsmeyer-Peppas constant n = Exponent of release
Weibull	$\frac{Q}{Q_\infty} = 1 - e^{-bt^a}$	a = Shape parameter b = Scale parameter
Hopfenberg[a]	$\frac{Q}{Q_\infty} = 1 - (1 - k_{HF}t)^2$	k_{HF} = erosion constant[b]
General terms	Q = Mass of drug released at time, t Q_∞ = Total cumulative mass of drug released. t = time in minutes, min	

[a] For a cylindrical dosage form
[b] Normalized by initial drug concentration and initial radius of the dosage form.

2.4. Thermal properties

Thermal properties of drug-loaded chitosan methacrylate hydrogels were determined using Differential Scanning Calorimetry (DSC) (DSC 8000, Perkin Elmer, U.S.A.). LIDHCl and LIDHCl-loaded samples were heated from 25 to 200 °C while LVX and LVX-loaded samples were heated to 250 °C. The heating rate used was 10 °C min^{-1} and a nitrogen flow rate of 20 mL min^{-1} was used in all analyses.

2.5. Design of customized wound dressing structures

Wound dressing shapes were first designed in a CAD software (Autodesk® Inventor™) and exported as STL files. These STL files were then imported into a slicer software (PrusaSlicer, Prusa Research) in which, printing parameters such as the layer height, infill pattern and percentage infill were selected. The corresponding .gcode files were then generated and further modified by inserting additional .gcode commands to allow for the interchanging of nozzles to produce various drug-loaded hydrogel patterns in the wound dressings.

2.6. 3D printing of custom wound dressing structures

Drug-loaded chitosan methacrylate hydrogels were prepared as follows: 1% (*w/v*) of the drug (LIDHCl or LVX respectively) was dissolved along with 0.5% (*w/v*) LAP in DI water. 4% (*w/v*) lyophilized chitosan methacrylate was then dissolved in this solution under constant stirring until a homogenous gel was formed. The hydrogel was then added into 5 mL syringes, which were used to load 3 mL CELLINK® cartridges using a female–female luer lock. Cartridges were then centrifuged to remove air bubbles introduced during the mixing process.

The 3D printing of chitosan methacrylate wound dressings was carried out using the BIOX™ (CELLINK, Sweden) printer. The 3D printer has three printheads which allowed for up to three different drug-hydrogel formulations to be used to print a single wound dressing. A 25G conical nozzle was used and the printbed was set to room temperature. Printing pressures within the range of 50–150 kPa were used and the printbed speed was set to 15 mm s^{-1}. Freshly printed chitosan methacrylate wound dressings were then exposed to UV of wavelength 365 nm for 2 min to initiate the photo-crosslinking process.

2.7. In vitro drug release of drugs from various 3D printed wound dressing configurations

To simulate the release of drugs from the wound dressing to the wound bed during the actual application, all configurations were 3D-printed onto glass slides, which were then crosslinked before being subsequently placed into 50 mL centrifuge tubes containing 30 mL 1 x Phosphate Buffered Saline (pH 7.4). These centrifuge tubes were then placed in an incubator shaker operating at a temperature of 37 °C and a shaking speed of 150 rpm. At pre-determined time intervals, 1 mL of buffer was aliquoted and replaced with fresh buffer. Aliquoted buffers at

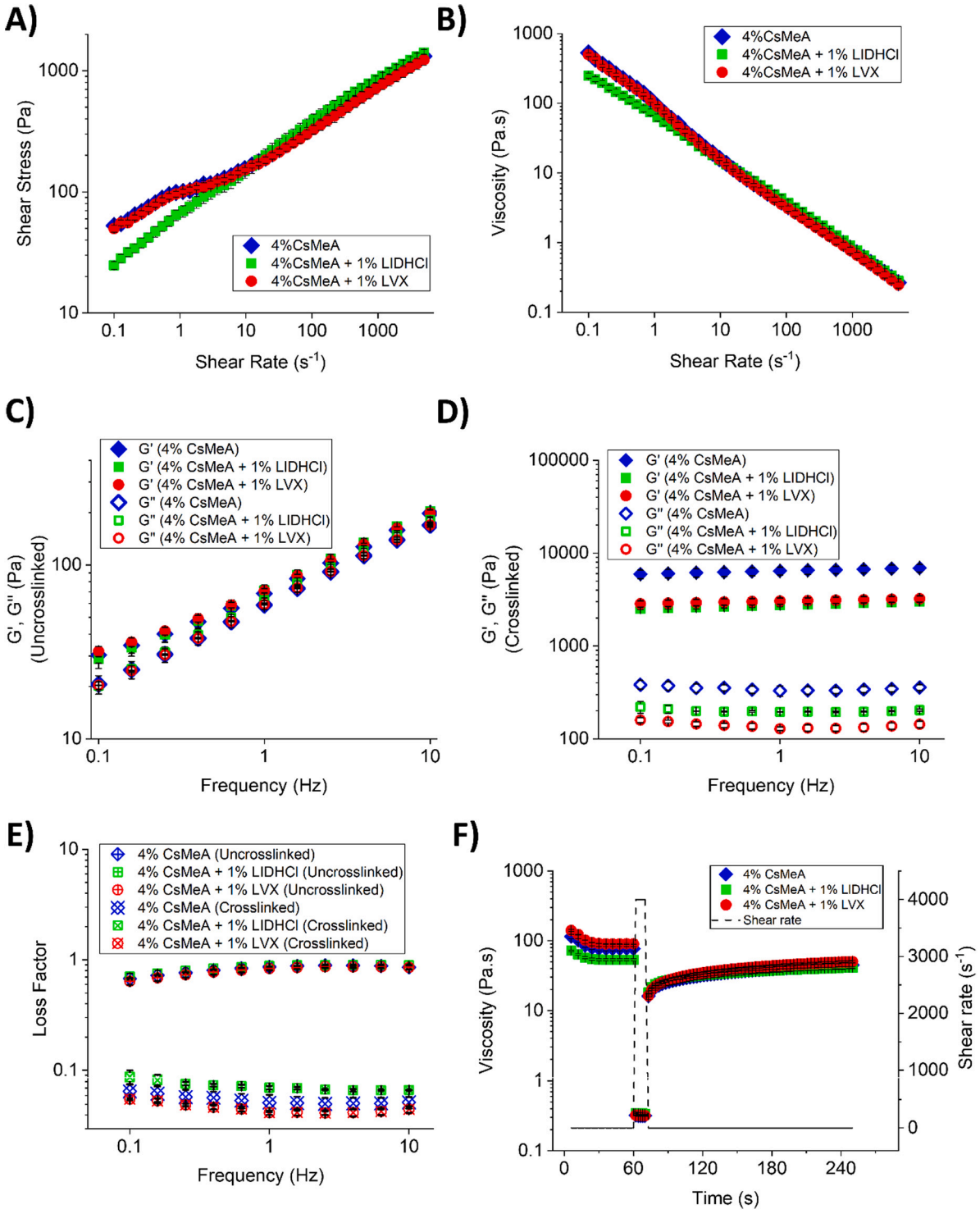

Fig. 1. Rheology profile of 4% (*w/v*) chitosan methacrylate (CsMeA) containing 0.5% (*w/v*) LAP and containing LIDHCl and LVX respectively. A) Shear stress profile of inks with respect to shear rate. B) Viscosity profile of inks with respect to shear rate. C) Storage and loss moduli of un-photo-crosslinked inks. D) Storage and loss moduli of photo-crosslinked inks. E) Loss factor of un-photo-crosslinked and photo-crosslinked inks. F) Thixotropic profile of inks.

all time points were then filtered and analyzed for their respective drug contents using High-Performance Liquid Chromatography (Prominence HPLC, Shimadzu, Japan). The HPLC was equipped with a C-18 reverse phase column (4.6×150 mm, 3.5 μm) (Kromasil Eternity CT 2.5, Nouryon, Netherlands) and UV-2487 UV-detector. The mobile phase used was Acetonitrile: 0.01 M phosphate buffer (60:40 *v/v*%, pH 7.4 ± 0.1, pH was adjusted using 0.1% (*v/v*) triethylamine). An injection volume of 10 μL was used. This experiment was performed in triplicates and results were expressed as mean±standard deviation.

2.8. Drug loading of drugs in various 3D printed wound dressings configurations

All configurations were 3D-printed onto glass slides, which were then placed into centrifuge tubes containing DI water without undergoing photo-crosslinking. Once the wound dressings were fully dissolved

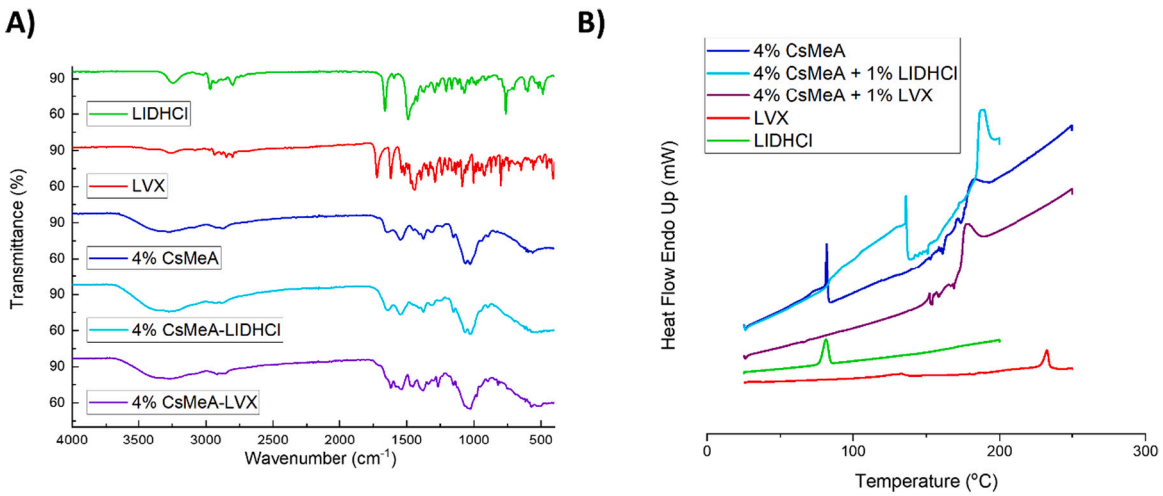

Fig. 2. A) FTIR spectra of chitosan methacrylate (CsMeA) containing LIDHCl and LVX respectively in comparison with the FTIR spectra of the individual base components. B) DSC graphs of chitosan methacrylate containing LIDHCl and LVX respectively in comparison with the graphs of the individual base components.

in DI water, aliquots were taken and diluted with Acetonitrile. The resulting solution was then filtered, and their respective drug contents were analyzed using HPLC. This experiment was performed in triplicates and results were expressed as mean±standard deviation.

2.9. Drug release kinetics

The drug release profiles of various 3D printed configurations were then fitted to the following drug release kinetic models: zero-order, first-order, Higuchi, Hixson-Crowell, Korsamayer-Peppas, Weibull and Hopfenberg. Table 1 presents equations for each model along with definitions of their respective terms. Each equation was normalized using the initial drug mass loaded in each wound dressing before fitting. For each release profile fitted, data points up until the saturation point were used in the fitting and the coefficient of determination (R^2) was used as a metric for comparison between different models.

3. Results and discussion

3D printing has been demonstrated to be capable of fabricating oral formulations containing tuneable dosages and release rates by modifying the shape of the excipient structure [36]. While 3D printing was also shown to be able to fabricate wound dressings for topical dosages [31,40,41], structures reported have yet to leverage the strengths of 3D printing in customizing structures and dosages as seen in oral dosages. Compared to oral dosages, the material used for the fabrication of wound dressings needs to be different considering the different routes of administration as well. While they share similar requirements such as the need to be biocompatible and biodegradable, excipients used for 3D printed oral dosages need to be impervious to the acidic conditions in the stomach in order to maintain the customized release profile as dictated by the structure of the excipient. Meanwhile, the material used for wound dressings for topical dosages should be soft and flexible enough to conform to the natural contours of the human body. It should also promote wound healing by either providing a moist wound environment, having products of biodegradation that can promote cellular proliferation and/or forming a protective barrier over the wound and protecting it from bacteria or other external stimuli. The post-processing step for oral dosages is also different compared to wound dressings. While 3D printed tablets need to be dried before use, hydrogel wound dressings can be applied either after lyophilization or in its hydrated gel form.

Here, we used chitosan methacrylate as the base component for our wound dressings. As a hydrogel, chitosan methacrylate has a high water content that does provide a moist wound environment for wound healing. It is also able to remove wound exudates. Chitosan methacrylate is also known in literature to be adhesive [44–46], which is a beneficial trait to have as a wound dressing [47]. With the presence of methacrylate groups and a photoinitiator, Chitosan methacrylate can undergo gelation relatively fast through UV photocrosslinking with negligible drug loss from the wound dressing as it does not require any exposure to solvents to undergo cross-linking. Meanwhile, LIDHCl and LVX are the drugs used in this study. LIDHCl is a common topical analgesic that relieves pain by blocking sodium channels in injured nerves. LVX is a third-generation quinolone that works by inhibiting the enzymes bacterial topoisomerase IV and DNA gyrase which are required for DNA replication, transcription, repair and recombination in bacteria [48]. Considering its known effectiveness towards the inhibition of common bacteria encountered in wounds [49], it has been prescribed for the treatment of skin infections, thus explaining its use in this study.

To determine its printability, the rheology of chitosan methacrylate was investigated. From Fig. 1A and 1B, chitosan methacrylate exhibits a shear-thinning behaviour under flow, as indicated by a decreasing viscosity profile with increasing shear rate. When loaded with LIDHCl and LVX respectively, a decrease in the maximum viscosity of the hydrogel was observed, indicating that both drugs have a plasticizing effect on chitosan methacrylate. The decrease in maximum viscosity caused by LIDHCl was found to be greater than LVX. At high shear rates though, the viscosities of chitosan methacrylate and both drug-loaded chitosan methacrylate hydrogels were similar. Nevertheless, the viscosities of all the drug-hydrogel formulations were still sufficiently high and the shear-thinning nature of the hydrogel was still preserved even after the addition of both drugs. This allows for the incorporation of LIDHCl and LVX without any compromise to the fabrication process.

Chitosan methacrylate at a concentration of 4% exists as a soft gel, as supported by its storage modulus being higher than its loss modulus prior to exposure to UV light (Fig. 1C). After photo-crosslinking, the storage modulus of chitosan methacrylate increased and the storage and loss moduli were also found to be less dependent on the oscillation frequency (Fig. 1D), indicating the formation of bonds between the methacrylate groups of different chitosan methacrylate chains. This also translates to a reduction in the loss factor (Fig. 1E). This reduction in loss factor was also demonstrated after photo-crosslinking formulations containing LIDHCl and LVX respectively, thus showing that the addition of either drug did not impede the photo-crosslinking process of the gel.

With respect to its thixotropy, chitosan methacrylate and drug-loaded chitosan methacrylate achieved a recovery ratio in the range of 16.2%–31.8% immediately after the excess shear was removed and the

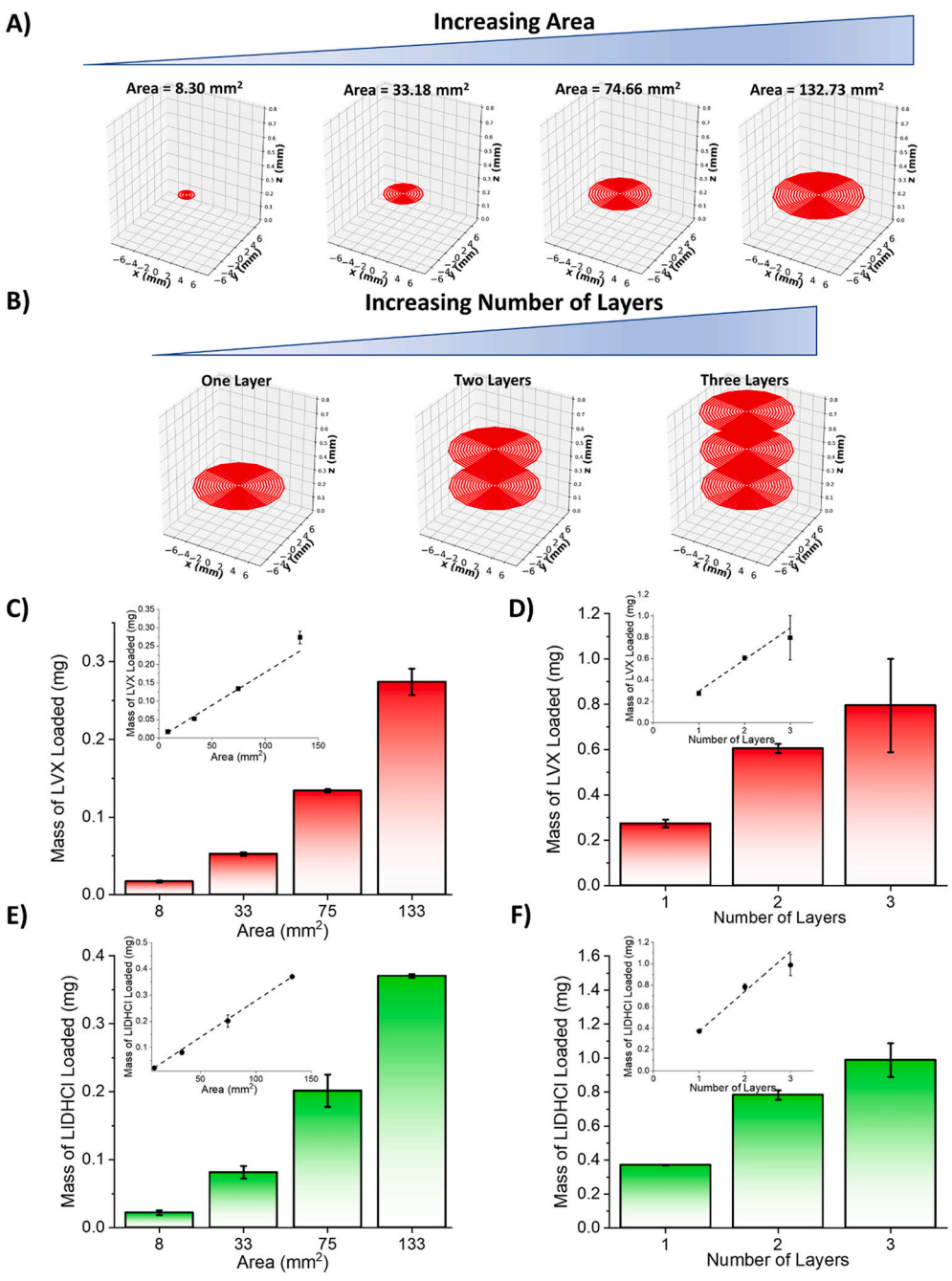

G)

R^2	LVX	LIDHCl
Area	0.9971	0.9999
Number of Layers	0.9981	0.9998

Fig. 3. A) Wound dressing designs of increasing area. B) Wound dressing designs of increasing height. C) Mass of LVX loaded with respect to the area of the wound dressing. D) Mass of LVX loaded with respect to the height of the wound dressing. E) Mass of LIDHCl loaded with respect to the area of the wound dressing. F) Mass of LIDHCl loaded with respect to the height of the wound dressing (inset: linear curve fitting of drug loaded with respect to area and height of wound dressing respectively). G) R^2 values of the mass of each drug loaded with respect to the area and height of the wound dressing respectively.

recovery ratio 3 min after the removal of the excess shear was in the range of 50.0%–72.5%. As such and as shown in Scheme 1, chitosan methacrylate maintained good shape fidelity after the removal of excess shear as wound dressings printed using 4% chitosan methacrylate were able to hold their respective shapes and configurations and did not sag or collapse during the printing process.

Owing to the moderate viscosity of the hydrogel used in this study and its nature as a soft gel during printing, there were few occurrences of nozzle clogging. Even when it did occur, it was resolved by simply purging the nozzle of any material between dressing fabrications by applying high pressure for a short period of time.

When incorporating drugs into the hydrogel matrix, we investigated if said drugs were reacting with the polymer chains and whether drugs were crystallizing inside the hydrogel matrix. The FTIR spectra in Fig. 2A show no additional peaks detected in drug-loaded hydrogels when compared to the spectrum for chitosan methacrylate, indicating that the drug was entrapped in the hydrogel matrix without reacting with any part of the chitosan methacrylate chain. The DSC graphs in

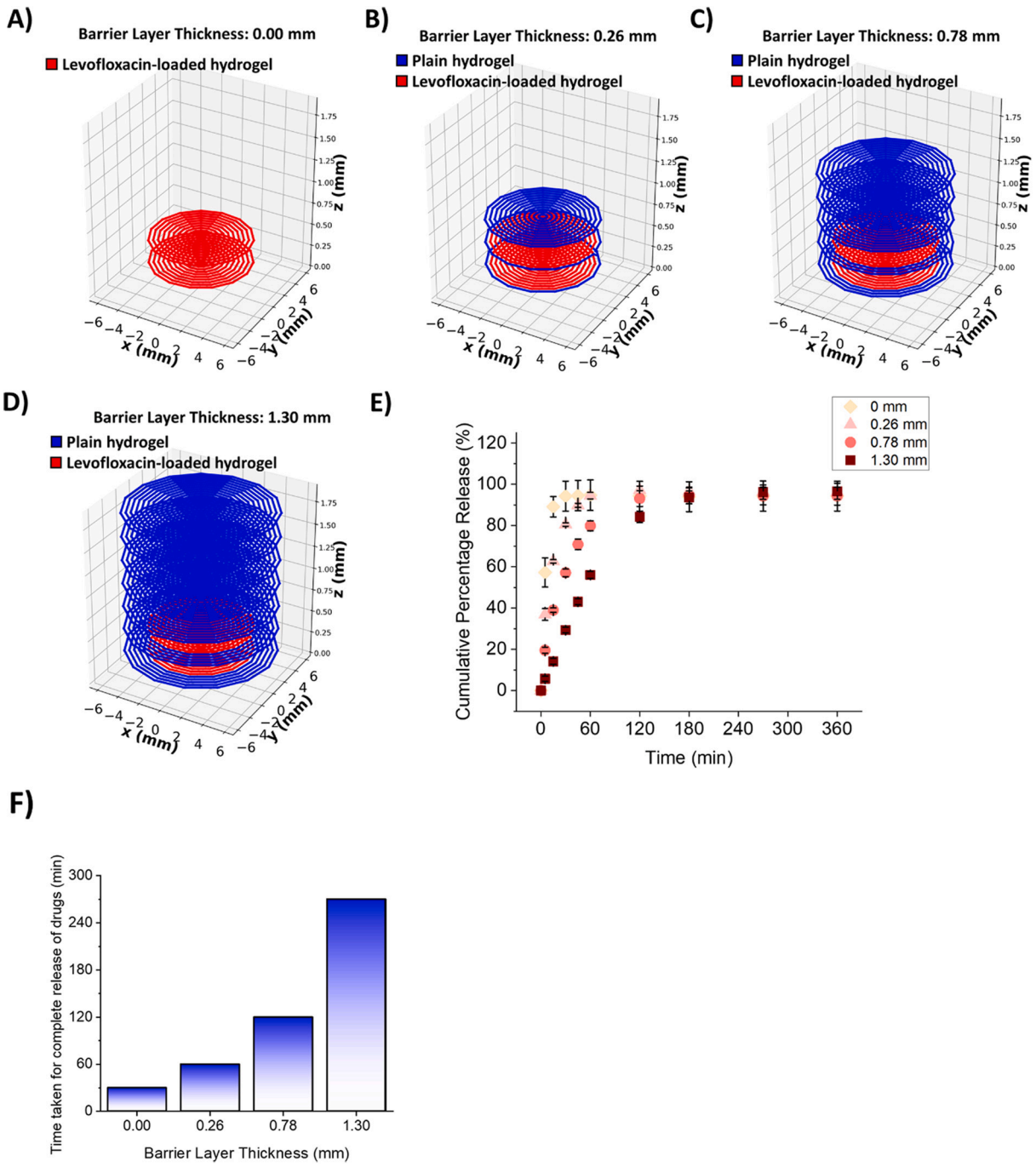

Fig. 4. Effect of various thickness of diffusion barrier layer [A) 0.00 mm, B) 0.26 mm, C) 0.78 mm and D) 1.30 mm] on E) the rate of release of LVX from 3D printed chitosan methacrylate wound dressing. F) The time taken for the complete release of LVX from each wound dressing design in A–D).

Fig. 2B indicate the absence of endothermic peaks found in the DSC curves of both drugs from their respective drug-filled hydrogels. This indicates the uniform distribution of both LIDHCl and LVX in the chitosan methacrylate hydrogel matrix respectively without any crystallization occurring. Thus, it is shown that both LVX and LIDHCl retain their respective functionalities when incorporated into chitosan methacrylate and are uniformly distributed throughout the wound dressing.

It can be assumed that besides LIDHCl and LVX, other drugs can also be used. However, as shown above, they must satisfy the following criteria: 1) The drug of choice should not have any undesired reaction with the hydrogel. 2) The drug of choice should not adversely affect the printability of the hydrogel by significantly changing its rheological properties. 3) The drug of choice must have sufficient solubility in water to achieve concentrations within the therapeutic window when released from the wound dressings. This ensures that the drug of choice remains stable and effective throughout the therapeutic window, thus preserving the overall efficacy of the wound dressing.

Considering the diverse shapes and configurations that can be created using 3D printing, we explored the correlation between drug dosage and the structure of the wound dressing. Fig. 3 shows the relationship between the mass of drug contained in a wound dressing and its area and number of layers respectively. Curve fitting shows that these relationships are linear with R^2 values greater than 0.99 for both area and number of layers for both drugs. This allows for the determination of drug content based on the structure of a particular wound dressing, provided that printing parameters remain constant. Having a linear

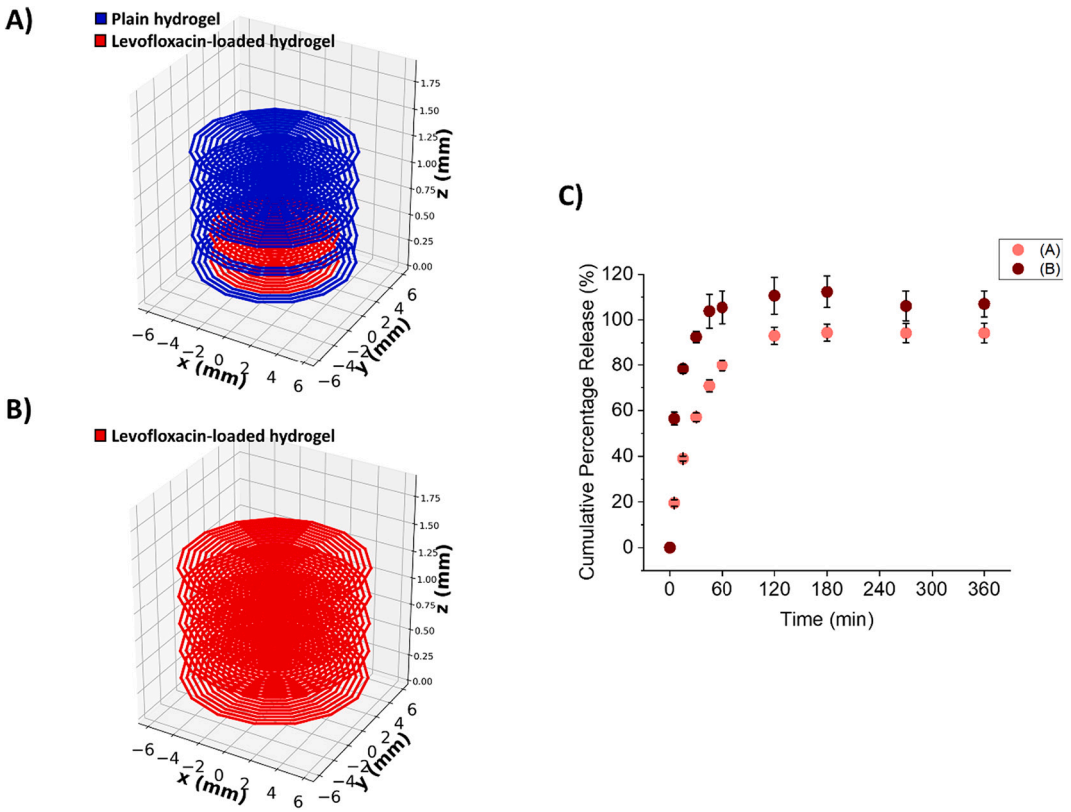

Fig. 5. A) Design of a wound dressing with a 0.78 mm thick barrier layer. B) Design of a wound dressing with the same dimensions as in A) but without the presence of any barrier layer. C) Cumulative release profile of LVX from both wound dressings.

correlation between the mass of the drug loaded and the area and number of print layers respectively also confirms the homogenous drug distribution in the hydrogel matrix as shown by the DSC curves (Fig. 2B), whereby the drug concentration is uniform throughout the entire area of the wound dressing.

Owing to the composition of hydrogels being mainly water, drugs will diffuse out of the dressing in a relatively small time frame. To overcome this, the effect of printing additional drug-free layers over drug-loaded layers was investigated for their ability to dampen the release of drugs from the wound dressing. From Fig. 4, having just a wound dressing comprise of the LVX-loaded compartment results in all the LVX being released in the first 30 min after administration. When an

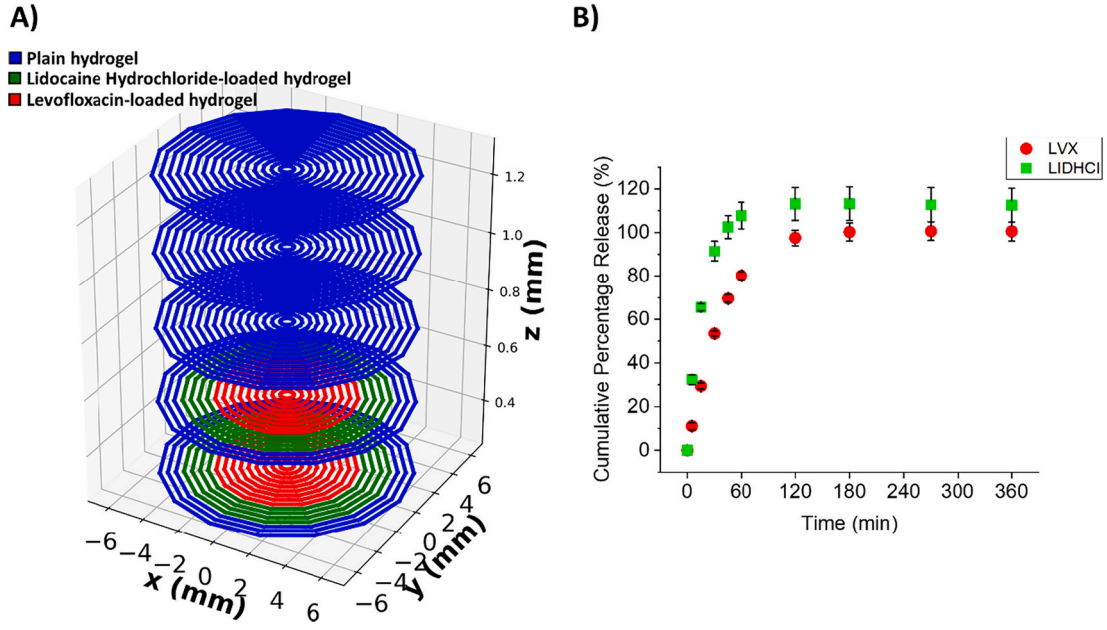

Fig. 6. A) Design of a wound dressing concurrently loaded with LVX and LIDHCl with the LVX-loaded layer and LIDHCl-loaded layer arranged in concentric circles of approximately equivalent volumes in the drug compartment. The drug compartment is surrounded by a 0.78 mm thick barrier layer. B) Cumulative release rate profile of both LIDHCl and LVX from the wound dressing design in A).

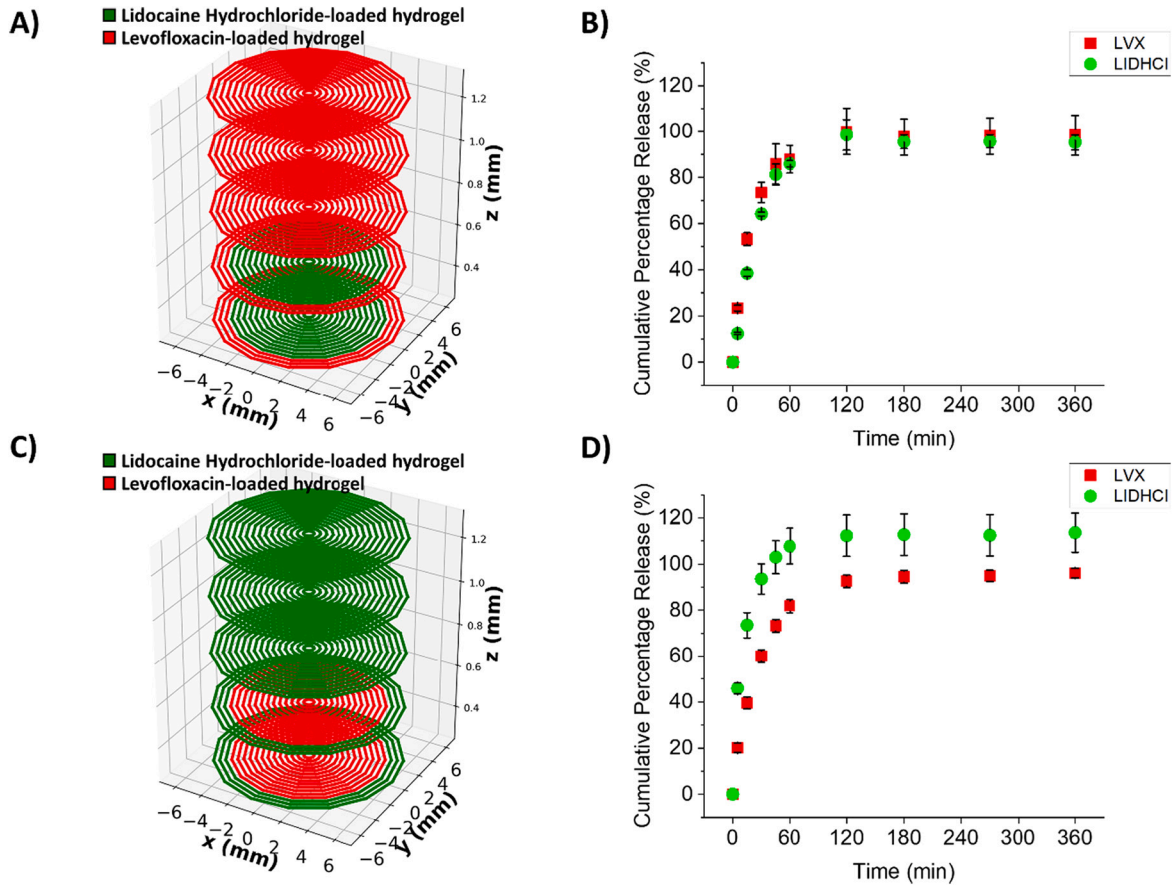

Fig. 7. A) Design of a wound dressing with LIDHCl in the drug compartment and LVX in the barrier layers. B) Cumulative release profile of both LVX and LIDHCl from the wound dressing design in A). C) Design of a wound dressing with LVX in the drug compartment and LIDHCl in the barrier layers. D) Cumulative release profile of both LVX and LIDHCl from the wound dressing design in C).

additional layer is printed around it, the duration of release was doubled, with all the LVX being released in the first hour after administration. Increasing the thickness of the barrier layer further dampens the release profile of LVX from the wound dressing and delays the release of most of the drugs, allowing for a more sustained release of LVX. With a barrier layer thickness of 1.30 mm, the duration of release was increased nine-fold compared to when there was no barrier layer covering the drug compartment. The dampening effect of the release profile can be attributed to the increase in the diffusion path, as a thicker barrier layer increases the distance between the drugs in the drug compartment of the wound dressing and the external environment.

Besides acting as a barrier to the diffusion of drugs from the wound dressing, drug-free hydrogel layers can also serve as a filler layer, in which the drug dosage can be tuned without compromising the intended shape and thickness of the wound dressing. Fig. 5 shows that printing the same shape using just drug-loaded hydrogel results in a higher dose of LVX. While the duration of release is longer than the wound dressing with just the drug compartment (Fig. 4A), having a barrier layer still allows the release duration to be more sustained. As an example, while having an initial high dosage of an antibiotic such as LVX is beneficial in eradicating bacteria, care must be taken to ensure that it is not administered in an amount that is cytotoxic to keratinocytes, fibroblasts and other cells residing in the skin. As such, 3D printing is also beneficial in introducing fillers that can modulate the quantity of the drug loaded without compromising on the intended structure.

Using 3D printing, we have shown that the concurrent loading of two drugs is possible (Fig. 6A), allowing for their simultaneous release from the wound dressing. When printed concentrically, the release profiles of both drugs from the wound dressing as shown in Fig. 6B are the same, showing a linear rate of release in the first two hours before tapering off soon after. Here, the dosages of LIDHCl and LVX in the drug compartment are approximately the same as the print area of LIDHCl has been calculated to be the same as the print area of LVX. The similarity between dosages is approximate as there will be slight deviations in the dosage owing to the construction of the wound dressing in a discrete manner, resulting in the division of area between LIDHCl and LVX being an approximate. We found the rate of release of LIDHCl to be faster than LVX, having approximately 70% of its initial mass released compared to 35% of the initial mass of LVX in the first half-hour. This is due to LIDHCl being more hydrophilic than LVX, which causes it to diffuse at a faster rate through the barrier layer [50]. This release profile of LVX shown in this configuration is also consistent with the drug release profile of a wound dressing containing just LVX with the same barrier thickness (Fig. 4C). This is beneficial as it allows for versatility in combining different drug-loaded hydrogels without the need to create a single multidrug-hydrogel mixture with specific drug compositions. Hypothetically, the wound dressing can accommodate a larger variety of dosages in this fashion using a printer with multiple printheads. However, as shown above, the hydrophobicity of each drug incorporated will need to be considered as it will have an influence on its rate of release from the wound dressing.

Next, we investigated the drug release profiles of wound dressings with various drugs in different layers. Doing so should allow for dosages to be customized and for the initial percentage released to be modified as well. As shown in Fig. 7, having a drug occupy the barrier layer results in a higher initial percentage release owing to the larger mass of drugs loaded and its closer proximity to the external environment. Such a design can be beneficial in specific situations. For example, having

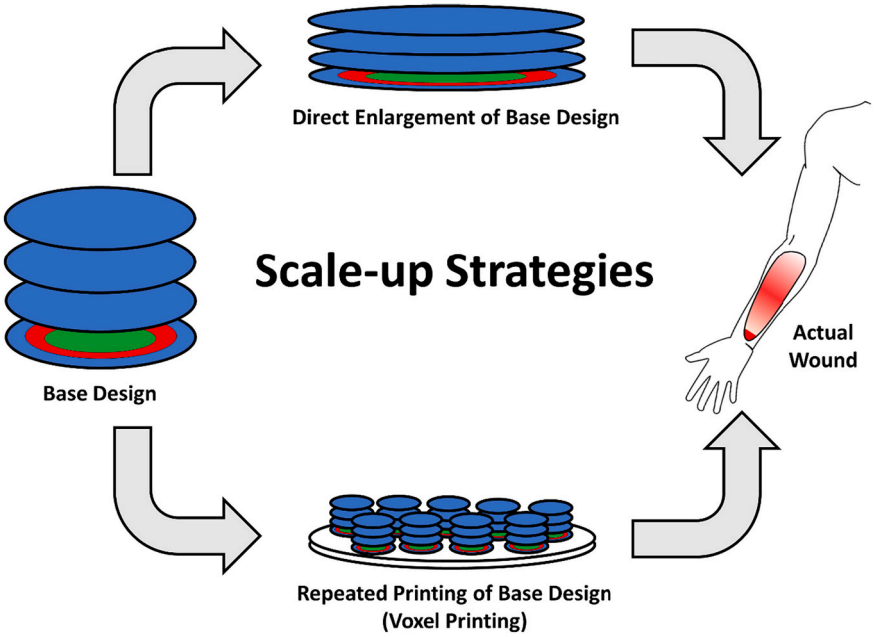

Scheme 2. Process scheme proposed for the scale-up of wound dressing designs proposed in this study to match the size and shape of wounds in a clinical setting. The base design can either be directly enlarged to fit the size and shape of the wound bed or it can be repeatedly printed as voxels on a template with the same shape and size as the wound bed.

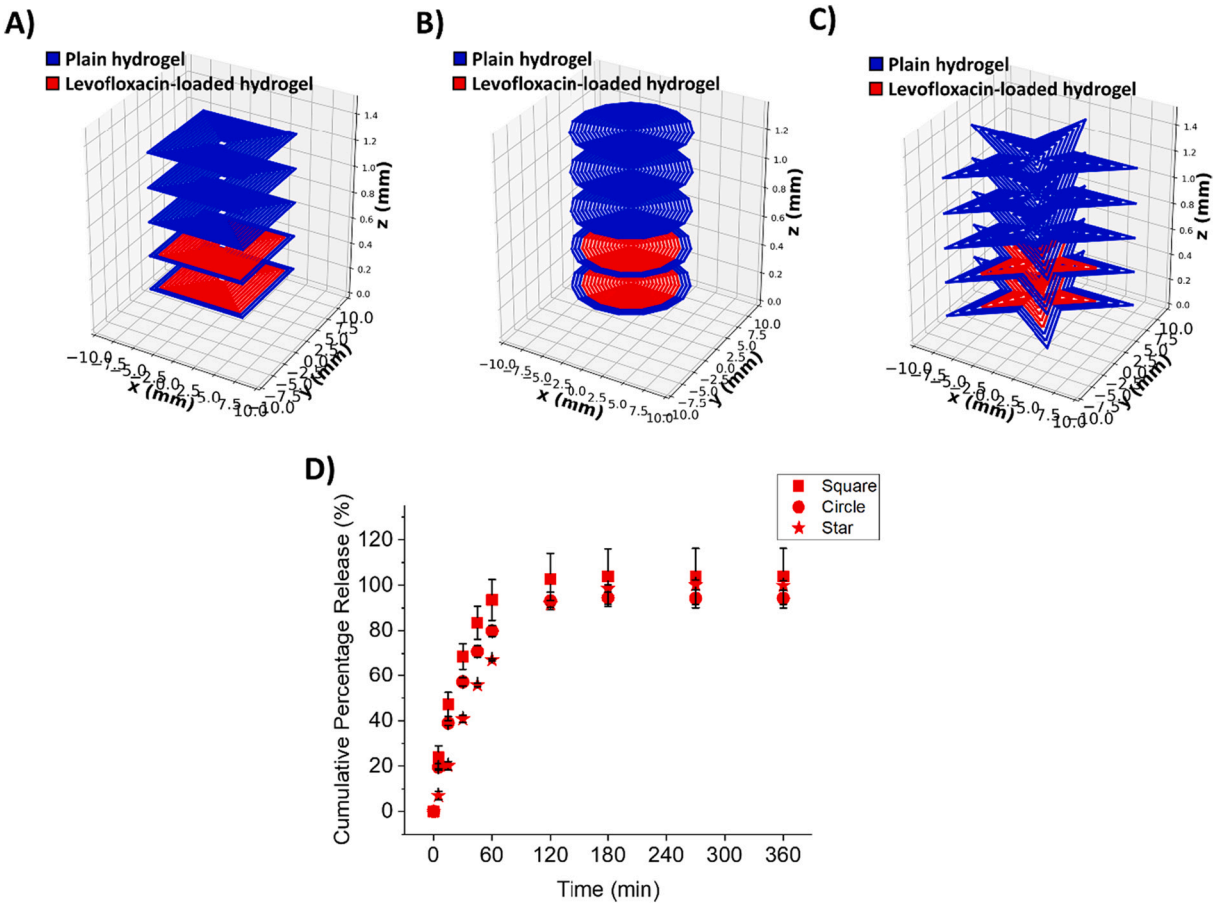

Fig. 8. Wound dressings with the shape of a A) square, B) circle and C) star respectively. The barrier layer thickness used for all three wound dressings is 0.78 mm. D) Cumulative release profile of LVX from all three wound dressings.

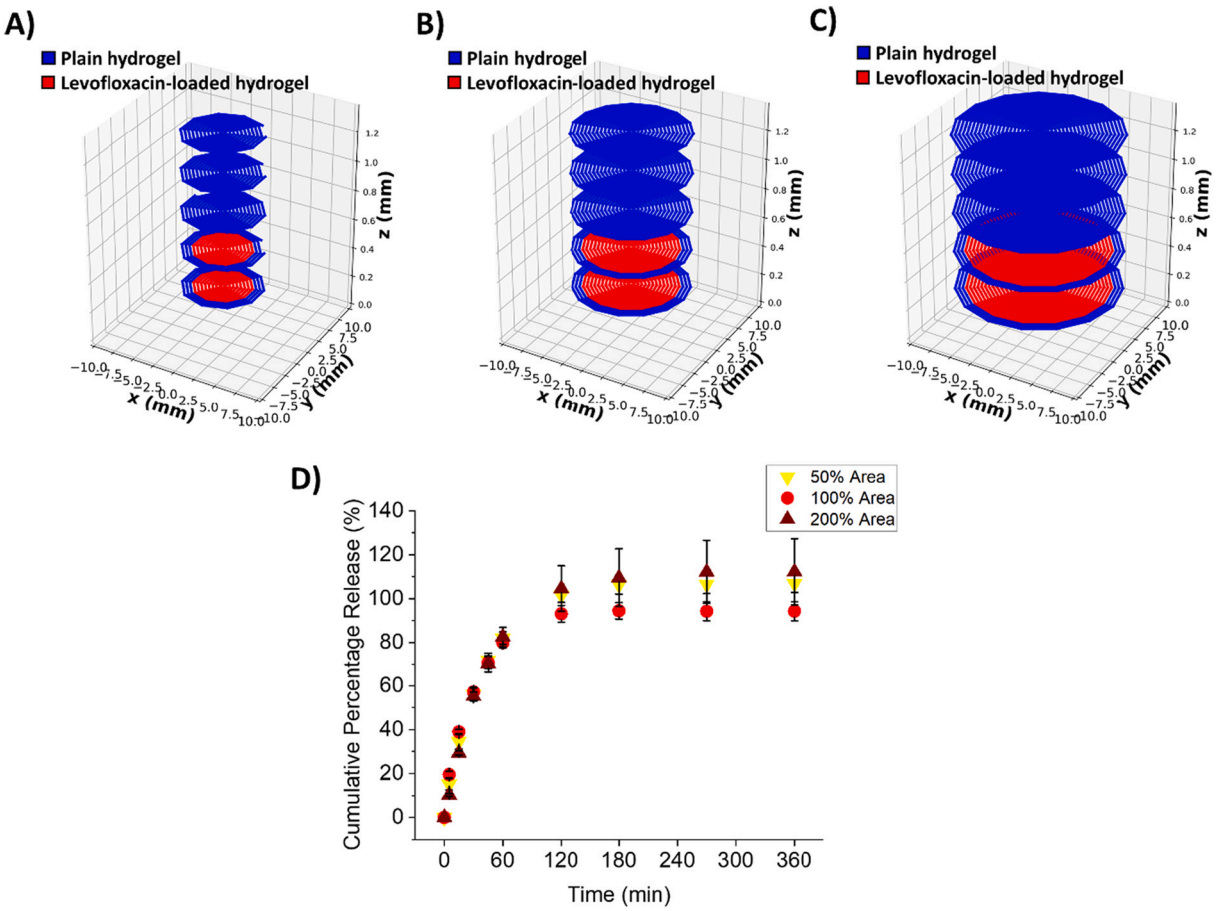

Fig. 9. Scaling up of wound dressings through direct enlargement. Wound dressings of various sizes (A) 50% of reference area, B) reference area, C) 200% of reference area). All wound dressings here have a barrier layer thickness of 0.78 mm. D) Cumulative release profile of LVX from all three wound dressings respectively.

LIDHCl in the barrier layer can provide greater pain relief if severe pain is diagnosed with a low incidence of bacterial infection. The opposite is true with LVX in the barrier layer and LIDHCl in the drug compartment. In the case of burn wounds, the former may be used for superficial burns while the latter can be used for deep partial-thickness burns, whereby patients are known not to feel pain due to the destruction of nerve endings at the wound site. In terms of dosages, as shown above, filler layers can also be included besides both LIDHCl and LVX loaded compartments to modulate the dosages of both drugs. Considering that LIDHCl diffuses out of the wound dressing at a faster rate than LVX, having a less hydrophilic drug in the outer layers will allow it to match the release rate and profile of more hydrophilic drugs loaded in the core of the wound dressing (Fig. 7B).

In a clinical setting, burn wounds are present in various shapes and sizes and thus, the release profiles provided by the customizable architecture of the wound dressing must be preserved with respect to changes in shape and size. Our proposed strategies to this are shown in Scheme 2. One strategy is to directly enlarge the base design to fit the size and shape of the wound (direct enlargement), while the other is to repeatedly print the original wound dressing architecture as voxels on a template that is of the same size and shape as that of the wound bed (voxel printing). As it has already been shown in Fig. 3 that the dosage per area of 3D-printed wound dressings is uniform, the scale-up process should not cause any significant changes to the drug release profile of the original design. Thus, we have investigated the effects of the size and shape of the wound dressing on the drug release profile.

Taking LVX as the main drug loaded into the wound dressings, we have looked at the release profile of drugs from wound dressings of various shapes (Fig. 8 A–C). Here, the shapes designed have the same overall volume which includes a barrier layer with a thickness of 0.78mm. From the cumulative release profile in Fig. 8D, LVX is released at approximately the same rate for both the circular and square wound dressings. However, LVX was released at a slightly slower rate from the star-shaped wound dressing. One possible reason for this discrepancy is the increased barrier thickness in the radial direction at the tip of the five points of the star due to the acute angles at the points. At the tips, plotting the coordinates in the .gcode file shows a five-fold increase in thickness at the points of the star compared to the base of the points. However, this effect is not as profound as increasing the overall barrier layer thickness as this apparent increase in the thickness of the barrier layer should only affect drug diffusion in the radial direction, which should be less prominent than drug diffusion in the axial direction. While the barrier thickness is shown to still be a dominant factor in modulating the release of drugs from the wound dressing, the release rate of drugs from the wound dressing still has a dependence on the surface area to volume ratio of the wound dressing and the existence of additional angles and curves in the geometry.

Next, we looked at both scale-up strategies introduced in Scheme 2. For the direct enlargement strategy, we took the wound dressing design in Fig. 9B and both shrunk it by 50% (Fig. 9A) and enlarged it by 100% (Fig. 9C) respectively. Here, the diffusion profile of LVX from the wound dressing remained the same, regardless of shape. While increasing the area results in a smaller surface area to volume ratio, the increase in this ratio is quite small and as such, it does not seem to have a significant effect on the release rate of LVX from the wound dressing.

Meanwhile, for the voxel printing strategy, we treated the wound dressing design in Fig. 9B as a single voxel (Fig. 10A) and fabricated another wound dressing with two voxels (Fig. 10B). We then compared

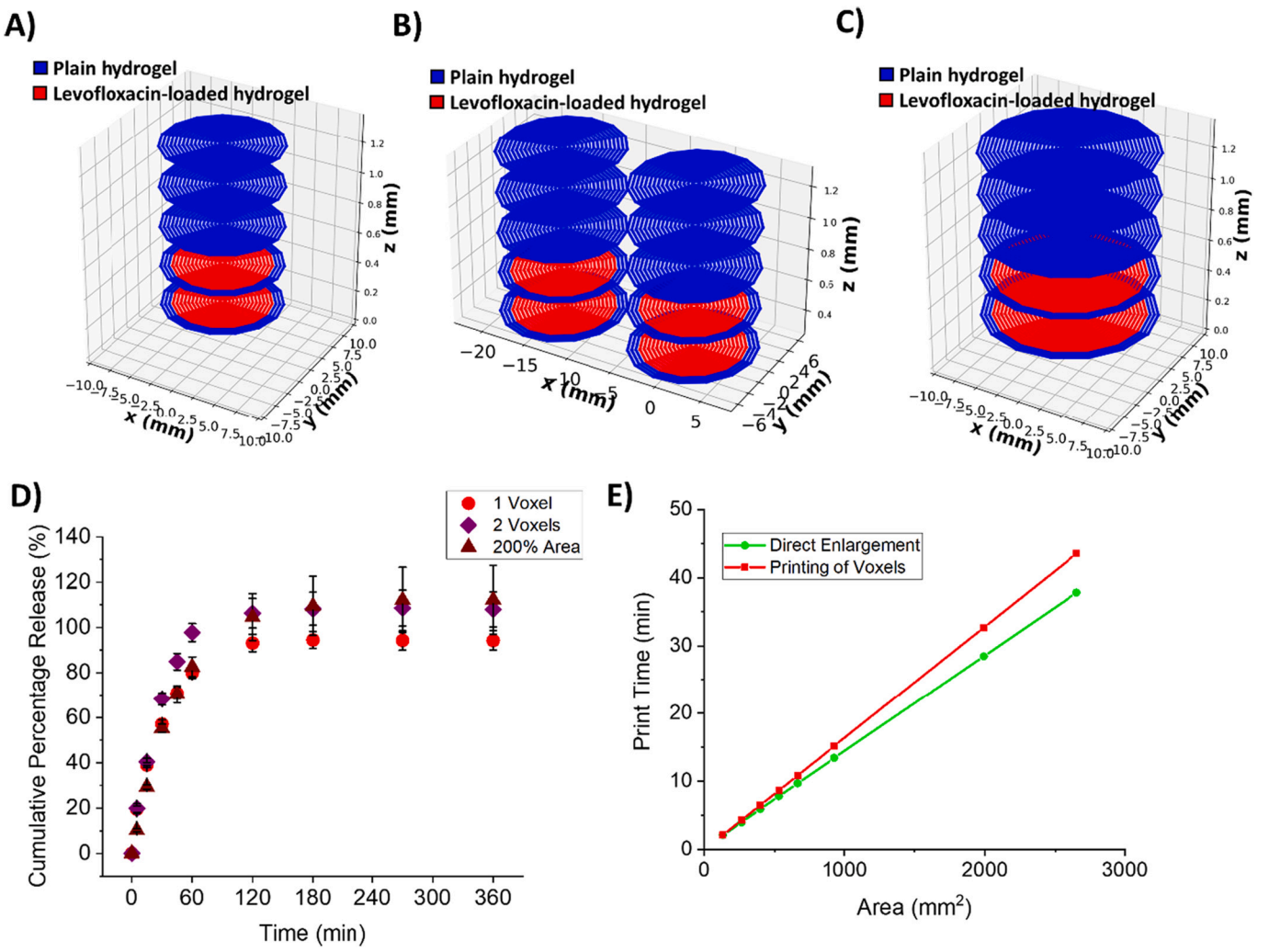

Fig. 10. Scaling up of wound dressings by replicating a single voxel throughout the entire area. A) Wound dressing with a single voxel with barrier layer of thickness 0.78 mm. B) Wound dressing with two voxels. C) Wound dressing that has double the area of a single voxel. D) Cumulative release profile of LVX from the wound dressings with a single voxel, double the area of a single voxel, and two voxels respectively. E) Comparison of print time between direct enlargement and voxel printing strategies respective with respect to increasing area of wound dressing.

its cumulative percentage release of LVX of both designs along with a wound dressing that was directly enlarged to have the same area as the wound dressing with two voxels (Fig. 10C). From the cumulative percentage release plots (Fig. 10D), LVX is shown to be released at a faster rate from the wound dressing with two voxels. Compared to when the base design was directly enlarged, the increase in surface area to volume ratio here is much greater, resulting in a more obvious increase in the rate of release of LVX. Besides comparing the rate of release of drugs from wound dressings scaled up using both strategies, we also looked at the time required to print wound dressings of increasing size using both strategies. From Fig. 10E, it is shown that due to the longer printing path required to print multiple copies of the original voxel, more time is needed to print the wound dressing when the voxel printing strategy is used. While the difference between the direct enlargement of the original design and printing the original design as voxels is negligible when the area required is small, this difference becomes more apparent when the area of the wound dressing required becomes larger, which is normally the case with burn patients with a high total body surface area.

Following our drug release studies, we then fitted various drug release kinetic models to the cumulative drug release profiles obtained in our study. A list of all the parameters of each model fitted to each cumulative drug release profile along with their respective coefficient of determinations is shown in Table 2. Graphical representations of comparisons between the plots of each actual and predicted cumulative drug release profiles are available in the supplementary material. Of all the models that were used to fit the release profiles for each configuration, the Zero Order and Hopfenberg models have a consistently poor fitting when compared with the other models. In contrast, most of the release profiles fitted best with the Weibull model, with one case having a slightly better fit with the first-order model and Korsmeyer-Peppas model respectively and the Hixson-Crowell model being a better fit for scaled-up wound dressings. Also, while not having the best fit for most cases in this study, the Korsmeyer-Peppas model fits relatively well to the drug release profiles, with R^2 values greater than 0.9 in all situations. As the thickness of the barrier layer increases, the shape parameter, a, in the Weibull model increases and becomes greater than 0.75 when the barrier layer reaches a certain thickness. This indicates the combination of Fickian diffusion with Case II transport. When a becomes greater than 1 as the thickness of the barrier layer increases further, drug transport out of the wound dressing becomes complex [51]. For all the models used, the constant term also decreases as the thickness of the barrier layer increases, confirming the dampening effect that the barrier layer has on the transport of drugs out of the wound dressing. When LIDHCl and LVX were concurrently loaded into the drug compartment, the constant term for the release profile of LIDHCl is always higher than that of LVX, thus describing the faster release of LIDHCl due to its more

Table 2
Parameters obtained from fitting the release kinetic models mentioned in Table 1 with the cumulative drug release profile from various wound dressing configurations in this study along with their respective R^2 values. Bolded parameters and R^2 values indicate the model with the best fit to a particular cumulative drug release profile from a particular wound dressing configuration.

Printing configuration		Zero order		First order		Hixson-Crowell		Higuchi		Korsmeyer-Peppas			Weibull			Hopfenberg	
		K_0	R^2	K_1	R^2	K_{HC}	R^2	K_H	R^2	K_{KP}	n	R^2	a	b	R^2	K_{HF}	R^2
Barrier thickness	0mm	0.0387	0.4889	0.1619	0.9944	0.0412	0.9768	0.1979	0.9070	0.3994	0.2642	0.9849	**0.7950**	**0.2397**	**0.9978**	0.0449	0.9392
	0.26mm	0.0196	0.5712	0.0644	0.9808	0.0174	0.9449	0.1355	0.9553	0.2330	0.3511	0.9925	**0.7186**	**0.1432**	**0.9959**	0.0217	0.9242
	0.78mm	0.0102	0.5123	0.0287	0.9887	0.0079	0.9692	0.0953	0.9640	0.1333	0.4189	0.9781	**0.7831**	**0.0610**	**0.9959**	0.0107	0.9641
	1.3mm	0.0062	0.8671	0.0133	0.9944	0.0038	0.9969	0.0688	0.9516	0.0368	0.6361	0.9766	**1.1603**	**0.0069**	**0.9982**	0.0053	0.9938
Concurrent loading of LIDHCl and LVX	LVX	0.0103	0.7133	0.0259	0.9987	0.0071	0.9985	0.0941	0.9653	0.0859	0.5219	0.9661	**1.0973**	**0.0182**	**0.9998**	0.0099	0.9967
	LIDHCl	0.0135	0.0831	0.0779	0.9736	0.0134	0.9224	0.1305	0.8382	0.2899	0.3059	0.9459	**1.0877**	**0.0613**	**0.9746**	0.0121	0.6015
LIDHCl in barrier layer	LVX	0.0103	0.4608	0.0305	0.9894	0.0084	0.9703	0.0969	0.9493	0.1443	0.4037	0.9700	**0.7903**	**0.0626**	**0.9956**	0.0110	0.9637
	LIDHCl	0.0136	-0.2097	0.1032	0.9711	0.0136	0.8195	0.1329	0.7510	0.3786	0.2443	0.9687	**0.8760**	**0.1398**	**0.9734**	0.0123	0.4202
LVX in barrier layer	LVX	0.0115	0.2607	0.0457	0.9935	0.0114	0.9669	0.1096	0.8959	0.2069	0.3458	0.9573	**0.8532**	**0.0725**	**0.9976**	0.0116	0.8558
	LIDHCl	0.0110	0.5384	**0.0339**	**0.9960**	0.0093	0.9953	0.1025	0.9353	0.1293	0.4439	0.9417	1.0785	0.0260	0.9956	0.0111	0.9678
Full loading of LVX		0.0135	-0.4762	0.1343	0.9655	0.0136	0.7029	0.1332	0.6462	**0.4568**	**0.1978**	**0.9831**	0.7213	0.2461	0.9768	0.0124	0.2581
Shape	Square	0.0116	0.3929	0.0420	0.9943	0.0111	0.9862	0.1099	0.9337	0.1785	0.3825	0.9662	**0.9248**	**0.0537**	**0.9956**	0.0114	0.8972
	Star	0.0069	0.7402	0.0182	0.9976	0.0050	0.9971	0.0778	0.9643	0.0664	0.5344	0.9663	**1.1375**	**0.0107**	**0.9999**	0.0069	0.9924
Size	50% Area	0.0078	0.4843	0.0287	0.9928	**0.0078**	**0.9963**	0.0908	0.9470	0.1329	0.4162	0.9638	1.0331	0.0255	0.9930	0.0077	0.8839
	200% Area	0.0079	0.5889	0.0274	0.9831	**0.0077**	**0.9963**	0.0915	0.9519	0.1101	0.4594	0.9554	1.1948	0.0135	0.9886	0.0075	0.9022
Voxels	2 Voxels	0.0119	0.5160	0.0403	0.9871	**0.0110**	**0.9960**	0.1114	0.9422	0.1484	0.4309	0.9522	1.1298	0.0261	0.9898	0.0112	0.9175

hydrophilic nature. Regarding the addition of drugs to the barrier compartment, the constant term of the drug in the barrier compartment is higher owing to the higher drug dosage and since the drugs in this compartment are in direct contact with the external environment, transport of drugs out of the wound dressing approaches Fickian diffusion, according to the Korsmeyer-Peppas equation. When scaling up, the rate constants appear to be independent of the area of the wound dressing, which seems to confirm that the transport of drugs out of the wound dressing is independent of the area of the wound dressing. However, they appear to differ depending on the shape of the wound dressing. The increase in the drug release rate from the wound dressing with two voxels was captured by the Hixson-Crowell model, with the constant term being higher than that for a wound dressing with one voxel and a wound dressing with double the area of that of a single voxel.

From this study, the use of 3D printing to fabricate wound dressings has been seen to fulfil some of the properties of an ideal antimicrobial dressing as described by Vowden and Cooper [52]. With 3D printing, wound dressings that conform to the size and shape of the wound can be fabricated while being cost-effective at the same time through the minimization of material wastage during fabrication. 3D printing is also able to customize the composition and design of wound dressings to satisfy patient and clinician expectations and the various designs highlighted in this article show that rapid but sustained activity can be achieved.

Similar to other studies involving the use of pneumatic extrusion for the fabrication of constructs using hydrogels, limitations encountered in this study include clogging in the nozzle as mentioned earlier, which may be due to the drying of the hydrogel at the tip from exposure to air. Again, this can be remedied by ensuring the inks are homogenous before printing and by either introducing a nozzle purge step or replacing the nozzle at regular intervals if disposable nozzles are used.

While the printing of a drug-free layer over the drug-loaded layer has been shown to prolong the rate of release of drugs out of the wound dressing, increasing the molecular weight of chitosan used in the synthesis step [53] or through the introduction of other printable materials with a higher diffusion coefficient such as thermoplastics [41] should be able to further increase the duration of release. The surface of the hydrogel wound dressing also has a significant role in controlling the diffusion of drugs to the wound bed. Besides the need to ensure sufficient contact between the surface of the wound dressing and the wound bed for effective delivery of drugs to the wound bed, the surface can also either impede or facilitate the diffusion of drugs from the wound dressing. As such, the diffusion of drugs to the wound bed can also be modulated through surface modification, in which an additional barrier layer is introduced. Through this modification, the hydrophobicity of the surface can be altered [54,55] and it can be made to swell or collapse in response to stimuli such as temperature (through grafting of thermosensitive polymers) [56,57] and pH (through grafting of polyelectrolytes) [55,56]. Added advantages of surface modification is the potential to improve adhesiveness and biocompatibility of the wound dressing. The potential formation of a skin layer during UV crosslinking of hydrogels may also affect the diffusion of drugs to the wound bed due to the higher degree of crosslinking that occurs at the surface due to the closer proximity of the surface to the UV source [58,59]. However, the formation process will need to be controlled so as for significant and tuneable skin layers to be formed in this manner.

Bed leveling and mapping are also crucial to ensure a uniform wound dressing structure as layer height will change at points where the bed is higher or lower. This becomes especially important as the area of the wound dressing increases. Quality control during the preparation of drug-loaded hydrogel mixtures prior to printing is also important as any changes in the composition will result in deviations in the printing parameters required for the production of wound dressings of consistent size and dosages. Appropriate storage conditions are also needed to ensure that drug-loaded hydrogels do not dry out especially if there is a

need for long-term storage.

4. Conclusions

In this study, we have shown the capability of 3D printing to fabricate chitosan methacrylate wound dressings with complex structures designed by a CAD program and subsequently, a slicer program. These complex structures allow for the tuneable release of drugs from the wound dressing and for the precise and tuneable loading of multiple drugs into the wound dressing. Through the addition of multiple drug-free layers around and above drug-loaded layers, drug diffusion out of the wound dressing from the drug-loaded layers can be dampened and tuned. The use of multiple printhead 3D printers allows wound dressings to be loaded with multiple drug dosages, providing flexibility for physicians to swap drugs in and out of the wound dressing according to their patients' needs. The location of each drug in different layers of the wound dressings can also be tuned to allow for different release rates. Out of all the drug release kinetic models used to fit the cumulative release profile from various architectures, the Weibull model had the best fit for most of the scenarios, with its parameters being able to quantitatively describe the effect that each architecture has on their respective cumulative drug release profiles. Meanwhile, the Hixson-Crowell model were marginally better in modelling drug release profiles in scaled-up dressings. Further studies will also need to be carried out in order to map structural and printing parameters and drug concentrations in hydrogels to the patient requirements. As mentioned previously, surface modification of the surface of the hydrogel is also another worthwhile endeavor to explore to complement the 3D printing process by providing greater control on drug transport out of the wound dressing. Another interesting future direction is to translate the layer-by-layer customizability directly to the filament itself through the use of coaxial needles and materials that can spontaneously crosslink upon contact with one another. Overall, this study serves as an insightful look into the ability of 3D printing to print wound dressings that are customizable in terms of shape, size, and composition.

Acknowledgement

This project is supported by NAMIC Singapore, NUS Centre for Additive Manufacturing (AM.NUS) and funded by the National Research Foundation Singapore under its Innovation Cluster Programme under the project number, 2018239 and grant number, R-279-000-577-592. Any opinions, findings and conclusions or recommendations expressed in this material are those of the authors and do not reflect the views of National Research Foundation, Singapore, NAMIC Singapore and AM.NUS. Jia Heng Teoh greatly appreciates the National University of Singapore Research Scholarship for the funding of his Ph.D studies in the National University of Singapore. The authors declare no conflict of interest.

Appendix A. Supplementary data

Supplementary data to this article can be found online at https://doi.org/10.1016/j.jconrel.2021.11.017.

References

[1] J.B. Shah, The history of wound care, J. Am. Col. Certif. Wound Spec. 3 (2011) 65–66.
[2] J.P. Junker, R.A. Kamel, E.J. Caterson, E. Eriksson, Clinical impact upon wound healing and inflammation in moist, wet, and dry environments, Adv. Wound Care (New Rochelle) 2 (2013) 348–356.
[3] B.S. Atiyeh, M. Costagliola, Cultured epithelial autograft (CEA) in burn treatment: three decades later, Burns 33 (2007) 405–413.
[4] R.J. Donegan, B.M. Schmidt, P.A. Blume, An overview of factors maximizing successful split-thickness skin grafting in diabetic wounds, Diab. Foot Ankle 5 (2014).
[5] R. Wiechula, The use of moist wound-healing dressings in the management of split-thickness skin graft donor sites: a systematic review, Int. J. Nurs. Pract. 9 (2003) S9–S17.
[6] M.R. El-Aassar, O.M. Ibrahim, M.M.G. Fouda, H. Fakhry, J. Ajarem, S.N. Maodaa, A.A. Allam, E.E. Hafez, Wound dressing of chitosan-based-crosslinked gelatin/polyvinyl pyrrolidone embedded silver nanoparticles, for targeting multidrug resistance microbes, Carbohydr. Polym. 255 (2021), 117484.
[7] Z. Gün Gök, M. Yiğitoğlu, İ. Vargel, Y. Şahin, M.E. Alçığır, Synthesis, characterization and wound healing ability of PET based nanofiber dressing material coated with silk sericin capped-silver nanoparticles, Mater. Chem. Phys. 259 (2021), 124043.
[8] K. Kalantari, E. Mostafavi, A.M. Afifi, Z. Izadiyan, H. Jahangirian, R. Rafiee-Moghaddam, T.J. Webster, Wound dressings functionalized with silver nanoparticles: promises and pitfalls, Nanoscale 12 (2020) 2268–2291.
[9] J. Jackson, H. Burt, D. Lange, I. Whang, R. Evans, D. Plackett, The design, characterization and antibacterial activity of heat and silver crosslinked poly(vinyl alcohol) hydrogel forming dressings containing silver nanoparticles, Nanomaterials (Basel) 11 (2021).
[10] M.T.S. Alcântara, N. Lincopan, P.M. Santos, P.A. Ramirez, A.J.C. Brant, H.G. Riella, A.B. Lugão, Simultaneous hydrogel crosslinking and silver nanoparticle formation by using ionizing radiation to obtain antimicrobial hydrogels, Radiation Phys. Chem. 165 (2019), 108369.
[11] R. Li, Z. Xu, Q. Jiang, Y. Zheng, Z. Chen, X. Chen, Characterization and biological evaluation of a novel silver nanoparticle-loaded collagen-chitosan dressing, Regen. Biomater. 7 (2020) 371–380.
[12] B. Mu, R. Wang, J. Gao, Z. Li, X. Li, Nano gold incorporated into *Aerva javanica* chitosan hydrogels disrupting agents against infections of burn wound, Mater. Technol. (2020) 1–10.
[13] V.T. A, A.K. Dinda, V. Koul, Evaluation of nano hydrogel composite based on gelatin/HA/CS suffused with Asiatic acid/ZnO and CuO nanoparticles for second degree burns, Mater. Sci. Eng. C Mater. Biol. Appl. 89 (2018) 378–386.
[14] G. Kowalski, M. Zawadzki, W. Leppert, P. Szpot, M. Siczek, K. Slowinski, M. Sobieszczanska, A. Gawlowska, K. Wieczorowska-Tobis, Analgesic efficacy of sufentanil in dressings after surgical treatment of burn wounds, Burns 47 (4) (2020) 880–887.
[15] E.M. Lima Junior, M.O. De Moraes Filho, B.A. Costa, A.V.P. Rohleder, M.B. Sales Rocha, F.V. Fechine, A.J. Forte, A. Alves, F.R. Silva Junior, C.B. Martins, M. B. Mathor, M.E.A. Moraes, Innovative burn treatment using tilapia skin as a xenograft: a phase II randomized controlled trial, J. Burn Care Res. 41 (2020) 585–592.
[16] S. Heilmann, S. Kuchler, C. Wischke, A. Lendlein, C. Stein, M. Schafer-Korting, A thermosensitive morphine-containing hydrogel for the treatment of large-scale skin wounds, Int. J. Pharm. 444 (2013) 96–102.
[17] B. Cheppudira, M. Fowler, L. McGhee, A. Greer, A. Mares, L. Petz, D. Devore, D. R. Loyd, J.L. Clifford, Curcumin: a novel therapeutic for burn pain and wound healing, Expert Opin. Investig. Drugs 22 (2013) 1295–1303.
[18] K. Shanmugapriya, H. Kim, H.W. Kang, EGFR-conjugated hydrogel accelerates wound healing on ulcer-induced burn wounds by targeting collagen and inflammatory cells using photoimmunomodulatory inhibition, Mater. Sci. Eng. C Mater. Biol. Appl. 118 (2021), 111541.
[19] C. Wiegand, P. Elsner, U.-C. Hipler, D. Klemm, Protease and ROS activities influenced by a composite of bacterial cellulose and collagen type I in vitro, Cellulose 13 (2006) 689–696.
[20] T.Y. Lu, K.F. Yu, S.H. Kuo, N.C. Cheng, E.Y. Chuang, J.S. Yu, Enzyme-crosslinked gelatin hydrogel with adipose-derived stem cell spheroid facilitating wound repair in the murine burn model, Polymers (Basel) 12 (2020).
[21] A. Oryan, E. Alemzadeh, A.A. Mohammadi, A. Moshiri, Healing potential of injectable *Aloe vera* hydrogel loaded by adipose-derived stem cell in skin tissue-engineering in a rat burn wound model, Cell Tissue Res. 377 (2019) 215–227.
[22] J. Xu, J.J. Xu, Q. Lin, L. Jiang, D. Zhang, Z. Li, B. Ma, C. Zhang, L. Li, D. Kai, H.-D. Yu, X.J. Loh, Lignin-incorporated nanogel serving as an antioxidant biomaterial for wound healing, ACS Appl. Bio Mater. 4 (2020) 3–13.
[23] K.M. Pasaribu, S. Gea, S. Ilyas, T. Tamrin, A.A. Sarumaha, A. Sembiring, I. Radecka, Fabrication and in-vivo study of micro-colloidal *Zanthoxylum acanthopodium*-loaded bacterial cellulose as a burn wound dressing, Polymers (Basel) 12 (2020).
[24] M.A. Mofazzal Jahromi, P. Sahandi Zangabad, S.M. Moosavi Basri, K. Sahandi Zangabad, A. Ghamarypour, A.R. Aref, M. Karimi, M.R. Hamblin, Nanomedicine and advanced technologies for burns: Preventing infection and facilitating wound healing, Adv. Drug Deliv. Rev. 123 (2018) 33–64.
[25] A. Awad, S.J. Trenfield, A. Goyanes, S. Gaisford, A.W. Basit, Reshaping drug development using 3D printing, Drug Discov. Today 23 (2018) 1547–1555.
[26] I. Gibson, D.W. Rosen, B. Stucker, Additive manufacturing technologies: Rapid prototyping to direct digital manufacturing, Springer, Boston, MA, 2010.
[27] S. Ramasamy, P. Davoodi, S. Vijayavenkataraman, J.H. Teoh, A. M. Thamizhchelvan, K.S. Robinson, B. Wu, J.Y.H. Fuh, T. DiColandrea, H. Zhao, E. B. Lane, C.-H. Wang, Optimized construction of a full thickness human skin equivalent using 3D bioprinting and a PCL/collagen dermal scaffold, Bioprinting 21 (2021), e00123.
[28] A.C. Daly, M.D. Davidson, J.A. Burdick, 3D bioprinting of high cell-density heterogeneous tissue models through spheroid fusion within self-healing hydrogels, Nat. Commun. 12 (2021) 753.
[29] Y. Wu, A. Wenger, H. Golzar, X.S. Tang, 3D bioprinting of bicellular liver lobule-mimetic structures via microextrusion of cellulose nanocrystal-incorporated shear-thinning bioink, Sci. Rep. 10 (2020) 20648.
[30] S. Cereceres, Z. Lan, L. Bryan, M. Whitely, T. Wilems, H. Greer, E.R. Alexander, R. J. Taylor, L. Bernstein, N. Cohen, C. Whitfield-Cargile, E. Cosgriff-Hernandez,

Bactericidal activity of 3D-printed hydrogel dressing loaded with gallium maltolate, APL Bioeng. 3 (2019), 026102.
[31] J. Long, A.E. Etxeberria, A.V. Nand, C.R. Bunt, S. Ray, A. Seyfoddin, A 3D printed chitosan-pectin hydrogel wound dressing for lidocaine hydrochloride delivery, Mater. Sci. Eng. C Mater. Biol. Appl. 104 (2019), 109873.
[32] H. Si, T. Xing, Y. Ding, H. Zhang, R. Yin, W. Zhang, 3D bioprinting of the sustained drug release wound dressing with double-crosslinked hyaluronic-acid-based hydrogels, Polymers (Basel) 11 (2019).
[33] H. Rastin, M. Ramezanpour, K. Hassan, A. Mazinani, T.T. Tung, S. Vreugde, D. Losic, 3D bioprinting of a cell-laden antibacterial polysaccharide hydrogel composite, Carbohydr. Polym. 264 (2021), 117989.
[34] Y.J.N. Tan, W.P. Yong, J.S. Kochhar, J. Khanolkar, X. Yao, Y. Sun, C.K. Ao, S. Soh, On-demand fully customizable drug tablets via 3D printing technology for personalized medicine, J. Control Release 322 (2020) 42–52.
[35] X. Xu, J. Zhao, M. Wang, L. Wang, J. Yang, 3D printed polyvinyl alcohol tablets with multiple release profiles, Sci. Rep. 9 (2019) 12487.
[36] Y. Yang, X. Wang, X. Lin, L. Xie, R. Ivone, J. Shen, G. Yang, A tunable extruded 3D printing platform using thermo-sensitive pastes, Int. J. Pharm. 583 (2020), 119360.
[37] Y. Jie Neriah Tan, W. Pong Yong, H. Low, J. Singh Kochhar, J. Khanolkar, L. Teng Shuen Ernest, Y. Sun, J. Zhi En Wong, S. Soh, Customizable drug tablets with constant release profiles via 3D printing technology, Int. J. Pharm. 598 (2021) 120370.
[38] Y. Sun, S. Soh, Printing tablets with fully customizable release profiles for personalized medicine, Adv. Mater. 27 (2015) 7847–7853.
[39] I. El Aita, J. Rahman, J. Breitkreutz, J. Quodbach, 3D-Printing with precise layer-wise dose adjustments for paediatric use via pressure-assisted microsyringe printing, Eur. J. Pharm. Biopharm. 157 (2020) 59–65.
[40] A. Goyanes, U. Det-Amornrat, J. Wang, A.W. Basit, S. Gaisford, 3D scanning and 3D printing as innovative technologies for fabricating personalized topical drug delivery systems, J. Control Release 234 (2016) 41–48.
[41] Z. Muwaffak, A. Goyanes, V. Clark, A.W. Basit, S.T. Hilton, S. Gaisford, Patient-specific 3D scanned and 3D printed antimicrobial polycaprolactone wound dressings, Int. J. Pharm. 527 (2017) 161–170.
[42] J. Dominguez-Robles, C. Mancinelli, E. Mancuso, I. Garcia-Romero, B.F. Gilmore, L. Casettari, E. Larraneta, D.A. Lamprou, 3D printing of drug-loaded thermoplastic polyurethane meshes: a potential material for soft tissue reinforcement in vaginal surgery, Pharmaceutics 12 (2020).
[43] H. Li, Y.J. Tan, K.F. Leong, L. Li, 3D bioprinting of highly thixotropic alginate/methylcellulose hydrogel with strong interface bonding, ACS Appl. Mater. Interfaces 9 (2017) 20086–20097.
[44] M. Diolosa, I. Donati, G. Turco, M. Cadenaro, R. Di Lenarda, L. Breschi, S. Paoletti, Use of methacrylate-modified chitosan to increase the durability of dentine bonding systems, Biomacromolecules 15 (2014) 4606–4613.
[45] O.M. Kolawole, W.M. Lau, V.V. Khutoryanskiy, Methacrylated chitosan as a polymer with enhanced mucoadhesive properties for transmucosal drug delivery, Int. J. Pharm. 550 (2018) 123–129.
[46] L. Wang, X. Zhang, K. Yang, Y.V. Fu, T. Xu, S. Li, D. Zhang, L.N. Wang, C.S. Lee, A novel double-crosslinking-double-network design for injectable hydrogels with enhanced tissue adhesion and antibacterial capability for wound treatment, Adv. Funct. Mater. 30 (2019).
[47] L. Zhang, M. Liu, Y. Zhang, R. Pei, Recent progress of highly adhesive hydrogels as wound dressings, Biomacromolecules 21 (2020) 3966–3983.
[48] A. Gutierrez, J.M. Stokes, I. Matic, Our evolving understanding of the mechanism of quinolones, Antibiotics (Basel) 7 (2018).
[49] N.T. Thet, D.R. Alves, J.E. Bean, S. Booth, J. Nzakizwanayo, A.E. Young, B. V. Jones, A.T. Jenkins, Prototype development of the intelligent hydrogel wound dressing and its efficacy in the detection of model pathogenic wound biofilms, ACS Appl. Mater. Interfaces 8 (2016) 14909–14919.
[50] Z. Li, J. Guan, Thermosensitive hydrogels for drug delivery, Expert Opin. Drug Deliv. 8 (2011) 991–1007.
[51] V. Papadopoulou, K. Kosmidis, M. Vlachou, P. Macheras, On the use of the Weibull function for the discernment of drug release mechanisms, Int. J. Pharm. 309 (2006) 44–50.
[52] P. Vowden, R.A. Cooper, An integrated approach to managing wound infection, European Wound Management Association (EWMA) Position Document: Management of Wound Infection, 2006, pp. 2–6.
[53] M.H. Hettiaratchi, A. Schudel, T. Rouse, A.J. Garcia, S.N. Thomas, R.E. Guldberg, T.C. McDevitt, A rapid method for determining protein diffusion through hydrogels for regenerative medicine applications, APL Bioeng. 2 (2018), 026110.
[54] K. Zhang, W. Yan, R. Simic, E.M. Benetti, N.D. Spencer, Versatile surface modification of hydrogels by surface-initiated, Cu(0)-mediated controlled radical polymerization, ACS Appl. Mater. Interfaces 12 (2020) 6761–6767.
[55] G. Chinga-Carrasco, K. Syverud, Pretreatment-dependent surface chemistry of wood nanocellulose for pH-sensitive hydrogels, J. Biomater. Appl. 29 (2014) 423–432.
[56] T.R. Hoare, D.S. Kohane, Hydrogels in drug delivery: progress and challenges, Polymer 49 (2008) 1993–2007.
[57] R. Yoshida, K. Sakai, T. Ukano, Y. Sakurai, Y.H. Bae, S.W. Kim, Surface-modulated skin layers of thermal responsive hydrogels as on-off switches: I. Drug release, J. Biomater. Sci. Polym. Ed. 3 (1991) 155–162.
[58] M.H. Godinho, A.C. Trindade, J.L. Figueirinhas, L.V. Melo, P. Brogueira, A. M. Deus, P.I. Teixeira, Tuneable micro- and nano-periodic structures in a free-standing flexible urethane/urea elastomer film, Eur. Phys. J. E. Soft Matter 21 (2006) 319–330.
[59] J. Gu, X. Li, H. Ma, Y. Guan, Y. Zhang, One-step synthesis of PHEMA hydrogel films capable of generating highly ordered wrinkling patterns, Polymer 110 (2017) 114–123.